

Microfabricated devices for single objective single plane illumination microscopy (SoSPIM)

ELISA ZAGATO,^{1,2} TOON BRANS,^{1,2} STEVEN VERSTUYFT,³ DRIES VAN THOURHOUT,³ JEROEN MISSINNE,⁴ GEERT VAN STEENBERGE,⁴ JO DEMEESTER,¹ STEFAAN DE SMEDT,¹ KATRIEN REMAUT,¹ KRISTIAAN NEYTS,^{2,5} AND KEVIN BRAECKMANS^{1,2,*}

¹Laboratory of General Biochemistry and Physical Pharmacy, Ghent University, Belgium

²Center for Nano- and Biophotonics, Ghent University, Belgium

³Photonics Research Group, Department of Information Technology, Ghent University-IMEC, 9000 Gent, Belgium

⁴Centre for Microsystems Technology (CMST), Imec and Ghent University, Technologiepark, Belgium

⁵Liquid Crystals and Photonics Group, Ghent University, Belgium

*Kevin.Braeckmans@UGent.be

Abstract: Light sheet microscopy is a relatively new form of fluorescence microscopy that has been receiving a lot of attention recently. The strong points of the technique, such as high signal to noise ratio and its reduced photodamage of fluorescently labelled samples, come from its unique feature to illuminate only a thin plane in the sample that coincides with the focal plane of the detection lens. Typically this requires two closely positioned perpendicular objective lenses, one for detection and one for illumination. Apart from the fact that this special configuration of objective lenses is incompatible with standard microscope bodies, it is particularly problematic for high-resolution lenses which typically have a short working distance. To address these issues we developed sample holders with an integrated micromirror to perform single lens light sheet microscopy, also known as single objective single plane illumination microscopy (SoSPIM). The first design is based on a wet-etched silicon substrate, the second on a microfabricated polished polymer plug. We achieved an on-chip light sheet thickness of 2.3 μm (FWHM) at 638 nm with the polymer micromirror and of 1.7 μm (FWHM) at 638 nm with the silicon micromirror, comparable to reported light sheet thicknesses obtained on dedicated light sheet microscopes. A marked contrast improvement was obtained with both sample holders as compared to classic epi-fluorescence microscopy. In order to evaluate whether this technology could be made available on a larger scale, in a next step we evaluated the optical quality of inexpensive replicas from both types of master molds. We found that replicas from the polished polymer based mold have an optical quality close to that of the master component, while replicas from the silicon based mold were of slightly lower but still acceptable quality. The suitability of the replicated polymer based sample holder for single-lens light sheet microscopy was finally demonstrated by imaging breast cancer spheroids.

©2017 Optical Society of America

OCIS codes: (180.2520) Fluorescence microscopy; (180.6900) Three-dimensional microscopy; (350.3950) Micro-optics; (230.3990) Micro-optical devices; (220.4000) Microstructure fabrication.

References and links

1. "Method of the Year 2014," *Nat. Methods* **12**(1), 1 (2015).
2. J. Huisken and D. Y. Stainier, "Selective plane illumination microscopy techniques in developmental biology," *Development* **136**(12), 1963–1975 (2009).
3. M. Mickoleit, B. Schmid, M. Weber, F. O. Fahrbach, S. Hombach, S. Reischauer, and J. Huisken, "High-resolution reconstruction of the beating zebrafish heart," *Nat. Methods* **11**(9), 919–922 (2014).

4. V. Trivedi, T. V. Truong, A. Trinh, D. B. Holland, M. Liebling, and S. E. Fraser, "Dynamic structure and protein expression of the live embryonic heart captured by 2-photon light sheet microscopy and retrospective registration," *Biomed. Opt. Express* **6**(6), 2056–2066 (2015).
5. N. Vladimirov, Y. Mu, T. Kawashima, D. V. Bennett, C. T. Yang, L. L. Looger, P. J. Keller, J. Freeman, and M. B. Ahrens, "Light-sheet functional imaging in fictively behaving zebrafish," *Nat. Methods* **11**(9), 883–884 (2014).
6. M. B. Bouchard, V. Voleti, C. S. Mendes, C. Lacefield, W. B. Grueber, R. S. Mann, R. M. Bruno, and E. M. C. Hillman, "Swept confocally-aligned planar excitation (SCAPE) microscopy for high speed volumetric imaging of behaving organisms," *Nat. Photonics* **9**(2), 113–119 (2015).
7. F. Pampaloni, R. Richa, N. Ansari, and E. H. K. Stelzer, "Live Spheroid Formation Recorded with Light Sheet-Based Fluorescence Microscopy," in *Advanced Fluorescence Microscopy: Methods and Protocols*, J. P. Verveer, ed. (Springer New York, New York, NY, 2015), pp. 43–57.
8. F. Cella Zanacchi, Z. Lavagnino, M. Faretta, L. Furia, and A. Diaspro, "Light-Sheet Confined Super-Resolution Using Two-Photon Photoactivation," *PLoS One* **8**(7), e67667 (2013).
9. Z. Lavagnino, G. Sancataldo, M. d'Amora, P. Follert, D. De Pietri Tonelli, A. Diaspro, and F. Cella Zanacchi, "4D (x-y-z-t) imaging of thick biological samples by means of Two-Photon inverted Selective Plane Illumination Microscopy (2PE-iSPIM)," *Sci. Rep.* **6**, 23923 (2016).
10. U. Krzic, S. Gunther, T. E. Saunders, S. J. Streichan, and L. Hufnagel, "Multiview light-sheet microscope for rapid in toto imaging," *Nat. Methods* **9**(7), 730–733 (2012).
11. E. G. Reynaud, J. Peychl, J. Huisken, and P. Tomancak, "Guide to light-sheet microscopy for adventurous biologists," *Nat. Methods* **12**(1), 30–34 (2014).
12. J. G. Ritter, R. Veith, A. Veenendaal, J. P. Siebrasse, and U. Kubitscheck, "Light sheet microscopy for single molecule tracking in living tissue," *PLoS One* **5**(7), e11639 (2010).
13. H. Deschout, K. Raemdonck, S. Stremersch, P. Maoddi, G. Mermier, P. Renaud, S. Jiguët, A. Hendrix, M. Bracke, R. Van den Broecke, M. Roding, M. Rudemo, J. Demeester, S. C. De Smedt, F. Strubbe, K. Neyts, and K. Braeckmans, "On-chip light sheet illumination enables diagnostic size and concentration measurements of membrane vesicles in biofluids," *Nanoscale* **6**, 1741(2013).
14. R. Galland, G. Greci, A. Aravind, V. Viasnoff, V. Studer, and J. B. Sibarita, "3D high- and super-resolution imaging using single-objective SPIM," *Nat. Methods* **12**(7), 641–644 (2015).
15. S. Franssila, "Anisotropic Wet Etching," in *Introduction to Microfabrication* (John Wiley & Sons, Ltd, 2010), pp. 237–254.
16. E. Bosman, G. Van Steenberge, I. Milenkov, K. Panajotov, H. Thienpont, J. Bauwelinck, and P. Van Daele, "Fully Flexible Optoelectronic Foil," *Selected Topics in Quantum Electronics, IEEE Journal of* **16**(5), 1355–1362 (2010).
17. J. G. Ritter, R. Veith, J. P. Siebrasse, and U. Kubitscheck, "High-contrast single-particle tracking by selective focal plane illumination microscopy," *Opt. Express* **16**(10), 7142–7152 (2008).
18. K. Braeckmans, K. Buyens, W. Bouquet, C. Vervaeke, P. Joye, F. De Vos, L. Plawinski, L. Doeuvre, E. Angles-Cano, N. N. Sanders, J. Demeester, and S. C. De Smedt, "Sizing nanomatter in biological fluids by fluorescence single particle tracking," *Nano Lett.* **10**(11), 4435–4442 (2010).
19. B.-C. Chen, W. R. Legant, K. Wang, L. Shao, D. E. Milkie, M. W. Davidson, C. Janetopoulos, X. S. Wu, J. A. Hammer 3rd, Z. Liu, B. P. English, Y. Mimori-Kiyosue, D. P. Romero, A. T. Ritter, J. Lippincott-Schwartz, L. Fritz-Laylin, R. D. Mullins, D. M. Mitchell, J. N. Bembek, A.-C. Reymann, R. Böhme, S. W. Grill, J. T. Wang, G. Seydoux, U. S. Tulu, D. P. Kiehart, and E. Betzig, "Lattice light-sheet microscopy: imaging molecules to embryos at high spatiotemporal resolution," *Science* **346**(6208), 1257998 (2014).
20. F. O. Fahrbach, V. Gurchenkov, K. Alessandri, P. Nassoy, and A. Rohrbach, "Light-sheet microscopy in thick media using scanned Bessel beams and two-photon fluorescence excitation," *Opt. Express* **21**(11), 13824–13839 (2013).
21. M. Plöschner, V. Kollárová, Z. Dostál, J. Nyk, T. Barton-Owen, D. E. Ferrier, R. Chmelík, K. Dholakia, and T. Čížmár, "Multimode fibre: Light-sheet microscopy at the tip of a needle," *Sci. Rep.* **5**, 18050 (2015).
22. M. B. Ahrens, M. B. Orger, D. N. Robson, J. M. Li, and P. J. Keller, "Whole-brain functional imaging at cellular resolution using light-sheet microscopy," *Nat. Methods* **10**, 413 (2013).
23. M. Jemielita, M. J. Taormina, A. R. Burns, J. S. Hampton, A. S. Rolig, K. Guillemin, and R. Parthasarathy, "Spatial and Temporal Features of the Growth of a Bacterial Species Colonizing the Zebrafish Gut," *MBio* **5**(6), 01751 (2014).
24. J. C. Gebhardt, D. M. Suter, R. Roy, Z. W. Zhao, A. R. Chapman, S. Basu, T. Maniatis, and X. S. Xie, "Single-molecule imaging of transcription factor binding to DNA in live mammalian cells," *Nat. Methods* **10**(5), 421–426 (2013).

1. Introduction

While fluorescence microscopy offers high-contrast imaging in combination with selective labels, exposing biological samples to high intensity excitation light may lead to photobleaching of the fluorophores and induce phototoxicity to the cells or tissue under investigation. This problem is confounded when acquiring a 3-D stack of images, which

implies that the entire sample is illuminated during the acquisition of each image plane. Light Sheet Microscopy (LSM) was developed in response to these problems and was elected “Method of the Year 2014” by Nature Methods [1]. In a light sheet microscope, two perpendicular objective lenses are used, one for illumination and one for imaging. The illumination objective lens is used to project a thin sheet of excitation light in the sample in such a way that it coincides with the focal plane of the detection objective lens. By restricting excitation of fluorophores to the focal plane, intrinsic optical sectioning of the sample is achieved. To obtain 3-D images the sample is moved through the excitation light sheet along the detection optical axis. In this way each plane of the sample is illuminated only once, which reduces photobleaching and phototoxicity issues [2]. When combined with a fast camera, the technique is able to follow dynamic processes that are happening in (relatively) large 3D volumes, like the beating of the heart [3, 4] or the functioning of the brain [5, 6] of zebrafishes and mice, and live formation of spheroids [7]. Two-photon light sheet microscopy has been reported as well for improved imaging depth [8, 9]. However, widespread use of LSM is hindered due to the fact that it requires two perpendicular objective lenses [10] in close proximity with a dedicated sample holder in between [11, 12]. One problem is that such a configuration is not readily compatible with standard microscope bodies. A second disadvantage of such a configuration is that spatial constraints prohibit the use of high NA lenses which have short working distances.

In response to this need, microfabricated sample holders have been proposed that would enable high-resolution light sheet imaging in combination with standard microscope bodies [13, 14]. In the design proposed by Deschout et al. the sample holder is a disposable microfluidics chip made of a planar waveguide on a silicium or glass substrate. By butt coupling of a single mode optical fiber to the planar waveguide, a 9- μm -thick light sheet illumination could be achieved in the center of the microfluidic channel. While this sample holder was proven valuable for single particle tracking in biological fluids, it has limited use for imaging biological samples since the position of the light sheet is fixed. A more versatile design was recently proposed by Galland et al., which is based on a microfluidic chip with integrated 45° micromirrors. The chip is placed on a normal epi-microscope and a beam-shaping unit is used to provide a sheet of light that emerges from the microscope’s standard objective lens. After reflection on the 45° micromirror a horizontal sheet of light is obtained in the chip that coincides with the imaging focal plane of the same lens. With this configuration they managed to obtain single-lens LSM images of live embryos and super-resolution images of cell nuclei.

The microfabrication process of the master component for Galland et al.’s micromirror chip is based on sequential anisotropic wet etching and dry etching of a silicon wafer. Here we evaluate a less time consuming and less complex approach based on the polishing of an inexpensive polymer material at a 45° angle. After coating with aluminum or gold, we compare its optical performance to the Si chip according to Galland et al. in terms of thickness of the reflected light sheet (beam waist), the homogeneity along its optical axis (depth of field) and contrast achieved. Aimed at potential upscaling we additionally evaluated the optical performance of inexpensive replicas from both types of master molds. It is found that replicas from the polished polymer plug perform best and those are finally used for single-lens LSM imaging of breast cancer cells spheroids as an example application.

2. Chip design and fabrication

As described in more detail in the next section, the concept relies on the reflection of an elliptical Gaussian beam on a 45° micromirror to create a horizontal light sheet that coincides with the detection focal plane of the objective lens. Given the importance of the beam shape after reflection, we chose to compare two strategies to fabricate the tilted micromirror. In the first strategy, following a previously published method [15], the crystallographic properties of silicon were exploited and the mirror was made chemically flat by means of anisotropic

etching. For the second design the micromirror was fabricated by mechanically polishing a polymer sheet at 45 degree, which was then thinned to the required thickness [16]. Subsequently the sheet was coated by either a layer of gold or aluminum, known for their high reflectivity (85% for aluminum and >90% for gold at 45° incidence angle and $\lambda = 638$ nm). Aimed at upscaling towards inexpensive disposable devices, replicas are made as well by pressing the above mentioned master molds, referred to as “master components”, onto a transparent UV-curable polymer material to create a negative stamp. The negative stamp is then pressed on a UV-curable epoxy, cured and subsequently coated with a reflecting layer (Au or Al). In the sections below the fabrication process of these different micromirrors is described in detail.

2.1 Silicon micromirrors

The process to fabricate optically flat mirror walls into a silicon wafer is schematically depicted in Fig. 8 in Appendix A. It consists of three major steps, namely photolithography, etching and cleaning.

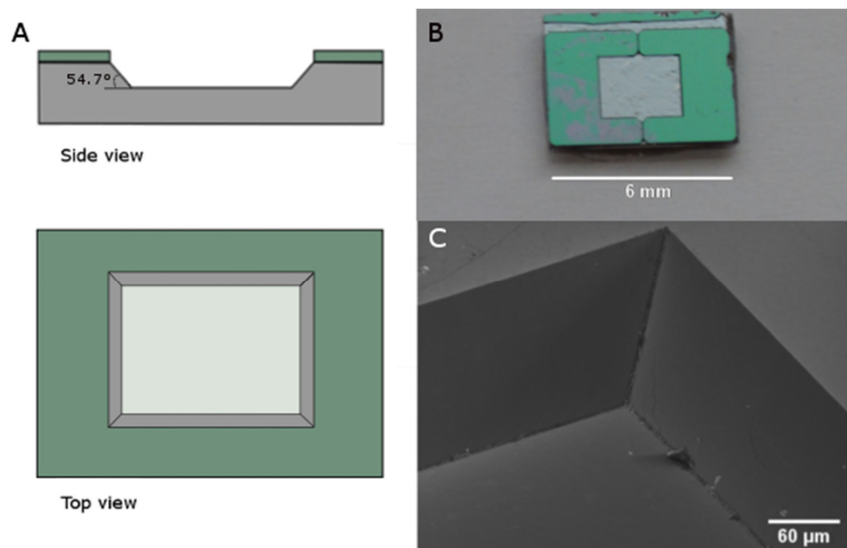


Fig. 1. Master mold with tilted micromirrors fabricated in silicon. (A) Schematic top and side view showing the microcavity with tilted micromirror walls into which the sample can be placed. (B) Top view picture of a microfabricated silicon master mold. (C) SEM micrograph showing the tilted walls of the master mold in one of the corners of the microcavity.

The wafer of choice is a thermo-oxidized wafer (silicon dioxide layer: 1 μm thick). After initial spin coating of a primer (TI Prime) and the positive photoresist az9260 (MicroChemicals GmbH, Germany), both followed by a 3 minutes baking step at 110°C, the wafer is covered with a chrome mask, that defines the position of the tilted walls and the channel, and subsequently exposed to UV light (Suss Microtech, Germany) for 200 seconds. The wafer is immersed for 90 s in an aqueous solution consisting of 1 part Developer 400K (MicroChemicals GmbH, Germany) and 2 parts distilled water in order to remove the UV illuminated regions of the photoresist. In the subsequent etching step, the wafer is placed for 16 min into a buffered 7:1 HF solution (MicroChemicals GmbH, Germany) that dissolves the unprotected regions of the silicon dioxide and exposes the underlying bare silicon. Next, the wafer is placed for 5 min in an ultrasonic bath filled with acetone to remove the photoresist layer. Then the wafer is put into a stirred KOH bath (KOH/Water/IPA 20/64/16) at 70°C that will selectively remove atoms in the $\langle 100 \rangle$ crystal direction, thus etching the channel with tilted walls at approximately 40 $\mu\text{m}/\text{hour}$. A careful monitoring of the etch rate by means of

temperature and concentration of the etchant is of the utmost importance since the etch rate can influence the wall roughness. Finally an RCA-1 clean was performed as follows. A solution of 5 parts water, 1 part 27% ammonium hydroxide and 1 part 30% hydrogen peroxide is heated at 70°C, then the wafer is soaked in the solution for 15 min, rinsed with water and put for 5 min into a 5% HCl solution. Figure 1 shows the end result of this process. In panel A the scheme of the silicon based master mold is portrayed. Panel B and panel C capture a picture of the silicon based master mold and a SEM micrograph of the tilted micromirror.

2.2 Polymer micromirrors

Optically flat tilted surfaces in polyimide (PI) were prepared as described in detail elsewhere [16]. A schematic description of the fabrication process is provided in Fig. 9 in Appendix A. Briefly, a 500- μm -thick flexible PI wafer (OPTIcomp Networks, Inc.) is clamped in a special PMMA device with a 45° trench. The whole device is polished to provide a 45° polished end facet to the PI foil. Subsequently, the edge defects from the polishing process are eliminated by thinning down the wafer to the desired thickness (200 μm in this case). Afterwards, the wafer is cut into small parts of the desired length and width by a wafer dicer with a diamond coated blade. The tilted end facets are then coated with a 120-nm-thin gold layer by vapor deposition, or with an aluminium layer applied by sputtering. The process yields thin micromirror plugs with an RMS roughness below 20 nm and good control over the angle (± 1 degree), see Figs. 2(a) and 2(c). A simple master mold is created by attaching two opposing mirror plugs to a glass microscope slide, as shown in Fig. 2(b).

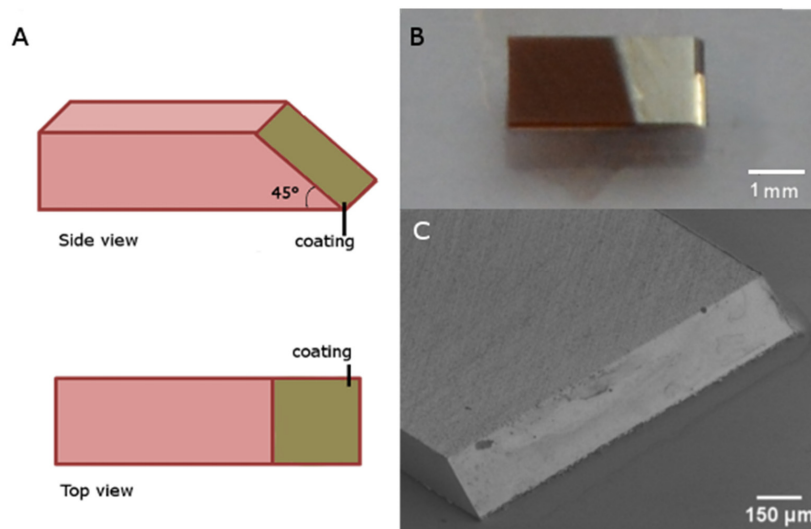


Fig. 2. Master mold with polished tilted micromirrors fabricated in polyimide. (A) Schematic top and side view of the polished polymer plug. (B) A simple master mold is created by gluing two of those polymer plugs, coated with aluminum (or gold), to a microscope slide. The sample can be placed in between the polymer plugs. (C) SEM micrograph of the polished polymer tilted mirror.

2.3 Disposable replicated sample holders

For imaging of biological specimen it is of interest to investigate the optical quality of inexpensive disposable replicas made from the master components. First, the polymer or silicon based master components are covered with a UV-curable, transparent fluorinated molding material (MD700, Solvay Solexis + photoinitiator). Following UV illumination, the polymerized material is easily peeled off from the master components. This stamp is then

used to fabricate the actual replicas. To this end, a drop of a UV-curable epoxy (EpoTek OG142-112) is dispensed on a glass slide and the molding stamp is pressed into the drop. Then the epoxy is cured using UV illumination and, after complete hardening, the molding stamp can be peeled-off. This results in epoxy structures with the same topology as the master components. In a final step the replicated micromirrors are coated with a 200 nm reflective layer of either gold (evaporation) or aluminum (sputtering). For a schematic description of the fabrication process, see Fig. 10 in Appendix A.

3. Optical setup

The excitation light sheet is provided by a laser source (Lasos RLD-638-150, λ : 638 nm, operating at 20 mW). To have full control of the waist, divergence, position and orientation of the light sheet in the measurement chamber, a custom-made beam shaping unit was built as schematically depicted in Fig. 3. After collimation, the beam passes three lenses (section S1) that serve as a variable beam expander. By choosing the appropriate distance between these lenses, the beam width at the back focal plane of the objective can be set, which in turn determines the waist thickness and divergence of the light sheet at the front focal plane of the microscope's objective lens (40x Nikon objective lens, CFI S Plan Fluor Brightfield, NA 0.6). A thin light sheet waist provides better contrast at the expense of more beam divergence and, therefore, a more limited field of view. Being able to choose the waist thickness make the sample holder more versatile and able to switch between observing small cells (thin light sheet and small field of view) and living organism (thicker light sheet and larger field of view).

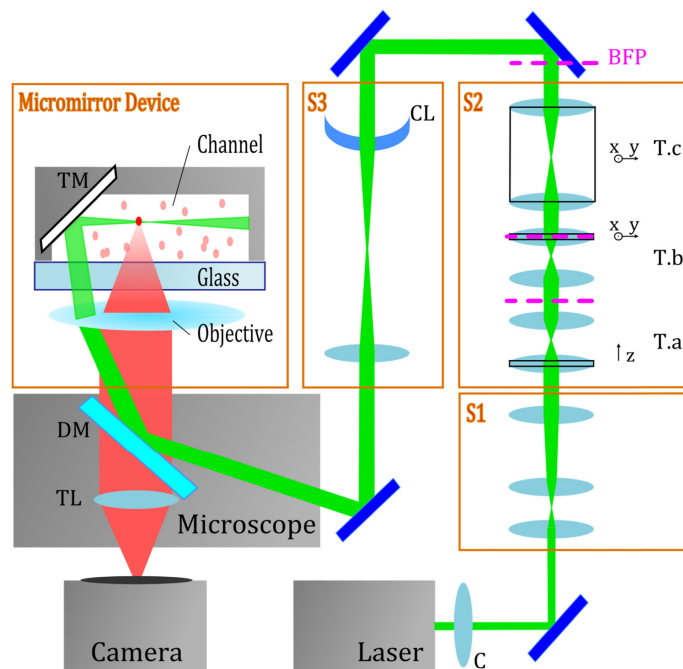


Fig. 3. Single lens light-sheet microscopy is achieved by reflection of an elongated elliptical Gaussian beam in a sample holder with integrated microfabricated tilted mirror (TM). After collimation (C), the laser beam passes through a variable beam expander consisting of three lenses (section S1), that allow to adjust the waist thickness and divergence of the light sheet in the channel. The light sheet focus in the sample holder is manipulated independently by the three telescopes (T.a, T.b and T.c) depicted in section S2. The laser beam is shaped into an elliptical Gaussian beam by a telescope in section S3 with a cylindrical back lens (CL). The fluorescent light emitted passes through a dichroic mirror (DM) and is imaged on the camera by a tube lens (TL).

Section S2 consists of three telescopes, each with a specific position with respect to a plane conjugated to the back focal plane of the microscope objective. Each telescope allows for an independent manipulation of the laser focus at the front focal plane of the objective lens: a translation of the laser focus along the axis of the beam, a lateral translation of the focus and a tilt of the laser beam with respect to the axis of the objective. These manipulations are achieved by respectively axially translating the back lens of the telescope T.a, laterally translating the front lens of T.b and jointly laterally translating both lenses of telescope T.c. After this, the beam passes section S3, consisting of a telescope with a cylindrical back lens. This produces an elliptical Gaussian beam in the focal plane of the objective lens. The laser beam is subsequently coupled into a microscope (Nikon Ti-E) onto which the sample holder with tilted micromirrors is installed. Fluorescence light coming from the sample is collected by the same objective lens and separated from the excitation light by a dichroic mirror. Images are acquired with a digital camera (iXon + , Andor, Belfast, UK).

4. Light sheet characterization and optical performance

4.1 Beam characterization and contrast using the master component

A first step in the comparison of the various micromirrors is the characterization of the light sheet beam profile after it is reflected by the micromirrors. At first, we wondered if the type of metal coating (gold applied through evaporation or aluminum applied through sputtering) would influence the optical quality of the reflected beam. As shown in Fig. 11 in Appendix B, neither the beam profile nor the achieved contrast are affected by the metal applied, thus both gold and aluminum can be used.

We first evaluated the optical quality of the reflected beam in both master components. The parameters that are of primary interest are the thickness of the light sheet (beam waist) and the homogeneity along its optical axis (effective depth of field). As it is not possible to visualize the light sheet from the side in the sample holders, we replaced the cylindrical lens (see Fig. 3) by a spherical one with the same focal length. In that way the focused beam can be easily visualized from the top through the microscope. A fluorescent solution of 10 μM ATTO647 was used to visualize the focused beam by fluorescence imaging. Figures 4(a) and 4(b) show the laser beam reflected from the silicon micromirror and from the polished polymer micromirror, respectively. The Full Width at Half Maximum (FWHM) of the focused beam along its optical axis is plotted in the graph in Figs. 4(c) and 4(d). We fitted the graph with the equation of propagation

$$W(x) = W_0 \sqrt{1 + \left(\frac{2x}{DoF_{eff}} \right)^2} \quad (1)$$

with W_0 the FWHM at the beam focus, proportional to the beam waist and DoF_{eff} the effective depth of focus. Parameters W_0 and DoF_{eff} were considered to be independent to account for a potential deviation of a perfect Gaussian beam propagation by optical aberrations induced by the micromirrors. The W_0 is determined as $2.4 \pm 0.3 \mu\text{m}$ for the polished polymer micromirror and $1.6 \pm 0.3 \mu\text{m}$ for the silicon micromirror. The corresponding DoF_{eff} was $19 \pm 0.3 \mu\text{m}$ and $10.0 \pm 1.0 \mu\text{m}$, respectively. Although the performance of both is quite similar, the slightly smaller beam waist with the silicon micromirror is likely due to its surface being more flat than that of the polished micromirror, as can be seen in Figs. 1(c) and 2(c).

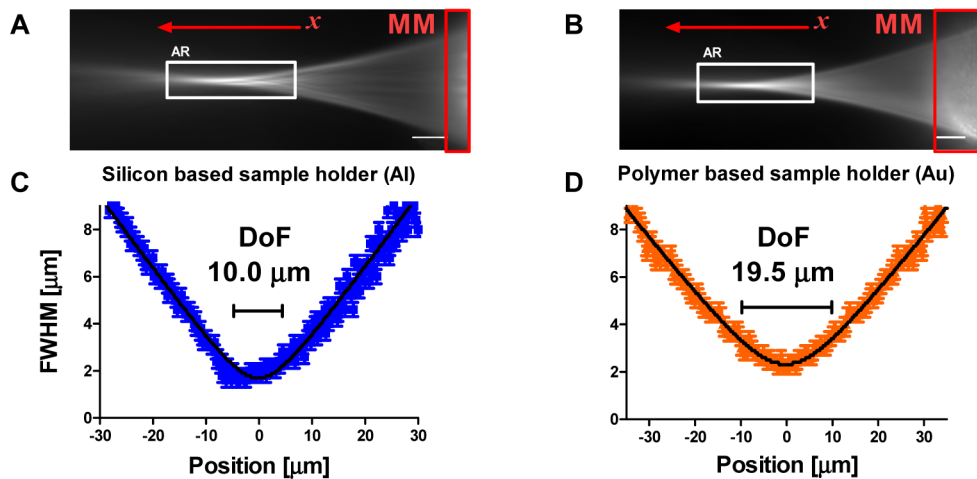


Fig. 4. Characterization of a beam reflected by the tilted micromirror in the silicon based mold (A) and the polymer based mold (B). The beam is imaged by filling the channel in both sample holders with a solution of $10 \mu\text{M}$ ATTO647. The red rectangles indicate the position where the excitation beam is reflected on the micromirrors (MM) while the white rectangle indicates the analyzed region (AR). The red arrows indicate the direction of the propagation of light. Scale Bar = $16 \mu\text{m}$. (C) and (D) The FWHM of the beam was determined along its optical axis in the analyzed region. The beam profile is fitted with Eq. (1) (black line). The silicon based mold had a beam waist of $1.6 \pm 0.3 \mu\text{m}$ (FWHM) and a DoF of $10.0 \pm 1.0 \mu\text{m}$. The polished polymer chip was found to have a beam waist of $2.4 \pm 0.3 \mu\text{m}$ (FWHM) and a depth of focus (DoF) of $19 \pm 0.3 \mu\text{m}$.

Another performance indicator is the contrast that is obtained for fluorescent samples. Similar to previous work [13, 17] we used fluorescent nanospheres (Invitrogen, dark red, diameter 100 nm) dispersed in red fluorescent solutions of Cy5 (Mirus Bio LLC, Madison, USA). The concentration of Cy5 was gradually increased to simulate an increasingly higher background intensity. The cylindrical lens was used to create a light sheet in the channel. Time-lapse videos of these samples (see [Visualization 1](#), [Visualization 2](#), [Visualization 3](#), [Visualization 4](#), [Visualization 5](#), [Visualization 6](#), [Visualization 7](#), [Visualization 8](#), and [Visualization 9](#)), were acquired and the contrast was determined for more than 300 of these nanospheres moving within the depth of field region using in-house developed particle tracking software [18]. The contrast C for every nanosphere is calculated from $C = (I - BG) / (I + BG)$, where I is the average intensity of the nanosphere and BG is the local background intensity calculated along a contour at 4 pixel distance around the edge of the nanosphere. The average contrast values are plotted in Fig. 5 as a function of Cy5 concentration. It is to be noted that more and more nanospheres become indistinguishable from the background as the concentration of Cy5 increases. The contrast for those invisible particles is put to zero in the calculation of the average contrast values. Thus, the average contrast was calculated presuming the same number of particles as registered in the videos without Cy5. The results in Fig. 5 are compared with the contrast values of the same nanospheres imaged with a home-build epi-fluorescent microscope [18]. The contrast obtained using light sheet illumination with the silicon- or the polymer- based mold is at least two times higher compared to epi-fluorescence microscopy.

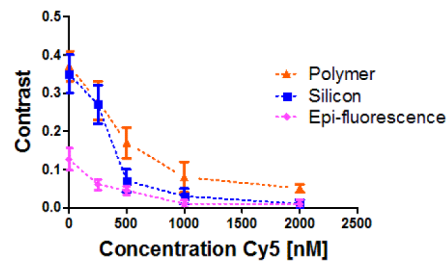


Fig. 5. Contrast comparison between light sheet illumination in the master component and epi-fluorescence illumination. Contrast was determined for fluorescent nanospheres suspended in solutions with increasing concentration of the red fluorescent dye Cy5. Measurements were performed in both molds and compared with normal epi-fluorescence imaging.

4.2 Beam characterization and contrast in the replicated sample holders

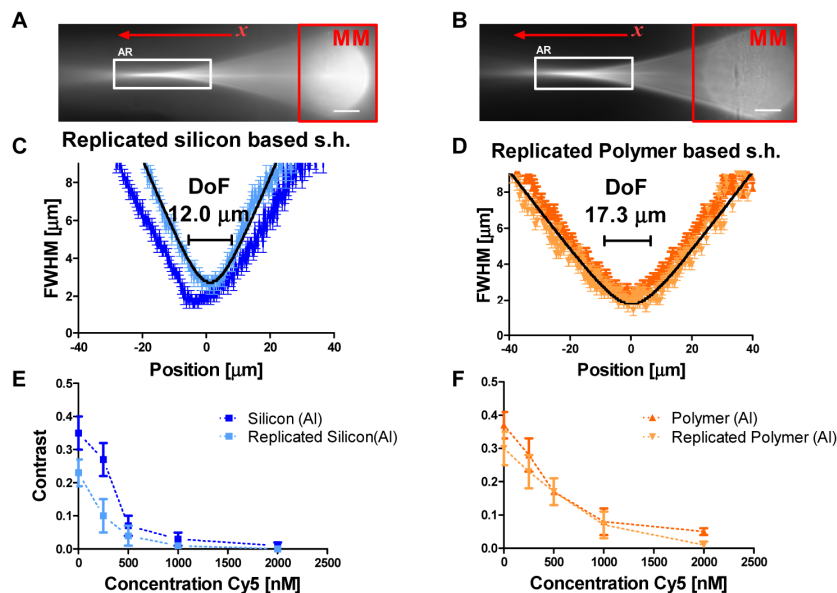


Fig. 6. Characterization of a beam in disposable sample holders replicated from the silicon (A) and polymer (B) based master mold. The beam is imaged by filling the channel in both sample holders with a solution of $10 \mu\text{M}$ ATTO647. The red rectangles indicate the position where the excitation beam is reflected on the micromirrors (MM) while the white rectangle indicates the analyzed region (AR). The red arrows indicate the direction of propagation of the light. Scale Bar = $16 \mu\text{m}$. (C, D) The FWHM of the beam was determined along its optical axis in the analyzed region indicated in figure A and B. The beam profile is fitted with the Eq. (1) (black line). The FWHM profile of the beam imaged using the replicated sample holder is compared to the profile obtained from the master components. The sample holder replicated from the silicon based master component was found to have a beam waist of $2.6 \pm 0.3 \mu\text{m}$ (FWHM) and a depth of focus (DoF) of $12.0 \pm 0.5 \mu\text{m}$. The sample holder replicated from the polished polymer master component had a beam waist of $1.9 \pm 0.3 \mu\text{m}$ (FWHM) and a DoF of $17.3 \pm 1.1 \mu\text{m}$. (E and F) Comparison between contrast measured in the replicated sample holders and in the master components of fluorescent nanospheres suspended in solutions with increasing concentration of Cy5.

As described in section 2.3, the silicon and polymer based sample holders are replicated in a UV-curable epoxy. The replicated sample holders, coated with aluminium, are tested and their performance in terms of beam profile and contrast achieved are compared to the performances of their master component in Fig. 6. Replicas from the silicon based mold show a rather asymmetric profile, see Fig. 6(c). The minimal FWHM W_0 is $2.6 \pm 0.3 \mu\text{m}$, that is, replicas

from the silicon based mold have a beam waist about 1.5 times wider than the beam waist of the master component. At the same time the DoF_{eff} enlarged slightly from 10.0 to 12.0 ± 0.5 μm . Replicas from the polymer based mold are found to have more regular beam profiles, see Fig. 6(d). Their W_0 , 1.9 ± 0.3 μm for the aluminium coated micromirror, is slightly better than the master component, which was 2.4 ± 0.3 μm . Correspondingly the DoF_{eff} decreased slightly from 19 to 17.3 ± 1.1 μm . This improvement could be due to small roughness's present in the master component that are smoothed out in the replication process. As a consequence, the contrast of replicated sample holders based on the silicon master mold in Fig. 6(e) is worse compared to the contrast observed in the silicon based master mold, while the contrast measured in the replicated sample holder based on the polymer master mold shown in Fig. 6(f) is comparable to the contrast measure in the polymer based master mold.

4.3 Imaging of spheroids

Following the successful fabrication and evaluation of the replicated polymer based sample holder, we finally demonstrate that it can be used for light sheet microscopy. eGFP positive MCF-7 human breast cancer cells were grown adherently until they reached 70% confluency, after which they were trypsinised and kept in suspension for 72h at 37°C, 5% CO₂ under constant gyratory shaking (70 rpm) to allow spheroid formation. The spheroids were then placed into the replicated sample holder and imaged in light sheet mode, shown in Fig. 7. The spheroid was imaged from bottom to top by moving the objective lens downward in 1 μm steps. This changes the incidence position of the illumination beam on the micromirror, so that the z-position of the horizontal light sheet in the microchannel is also changed. It is to be noted that this procedure also causes a lateral shift of the light sheet focus, which is compensated by appropriately adjusting the T.a telescope shown in Fig. 3. The difference in contrast is astounding in comparison with standard epi-fluorescent microscopy (see [Visualization 10](#)). In light sheet mode it is possible to identify single cells and their positions throughout the spheroid while this is not possible in the epi-fluorescence images. It demonstrates that high-quality light sheet imaging is possible with our sample holders replicated from the polymer master component.

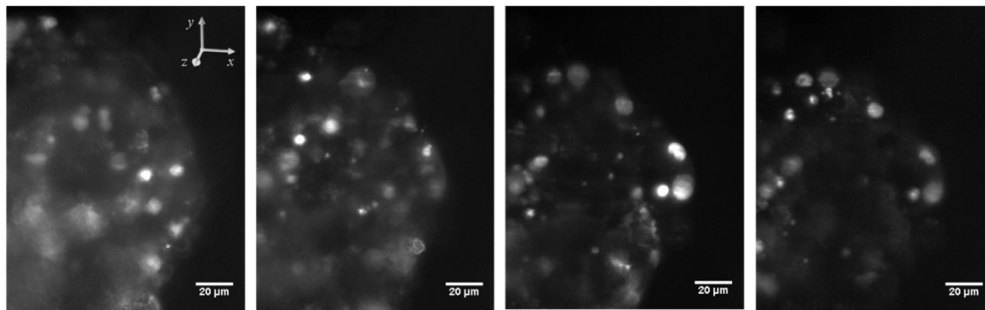


Fig. 7. Images of MCF-7 human breast cancer spheroids at different planes. Cells were imaged from bottom to top and the z-planes were 1 μm apart.

5. Discussion and conclusion

In recent years, the interest of the scientific community in light sheet microscopy has steadily increased and the field has seen many technological developments [19–21] as well as a tremendous rise in applications [7, 22, 23]. However, in its typical configuration LSM relies on at least two objective lenses that are placed orthogonally close to one another. For objective lenses with long working distances this is not a problem, but naturally this means that the numerical aperture, and therefore resolution, is limited. Therefore, for high resolution imaging, other solutions are required. In addition, such an orthogonal double lens

configuration is not easily compatible with standard microscopy bodies, thus hindering its widespread use in the biological community.

One solution consists of delivering the light sheet from the opposite direction of the detection lens and making use of a reflective surface close to the sample so as to reflect the light sheet horizontally into the sample. Leica, for instance, uses this approach in its commercial light sheet microscope. On an inverted microscope, they make use of two opposing 45° mirrors that are attached to the condenser lens of the diascope illumination arm. For light sheet imaging, the sample is mounted in hydrogel on a petri dish and the 45° mirrors are lowered so that they are placed around the gel-mounted sample. Laser light is coupled into the diascope illumination arm and is reflected horizontally. By rapid scanning of the laser beam in one direction, a light sheet is emulated in the sample and imaging is realized through the microscope's objective lens. While this configuration is well suited for imaging larger organisms, like e.g. *C. elegans*, it is not readily suited for imaging adherent cell cultures. An alternative solution was put forward by Gebhardt and his colleagues [24] who used a tipless AFM cantilever for horizontal reflection of the light sheet beam in adherent cell cultures. It allowed the use of high numerical aperture lenses and consequently the generation of a submicrometer light sheet, apt to illuminate single cells as close as $2\ \mu\text{m}$ from the coverslip. While a technological feat, this approach requires addition of specially manufactured AFM cantilever holder and separate optics to provide light sheet illumination incident onto the AFM cantilever, all mounted to a fluorescence microscope, which adds another layer of complexity.

A more practical approach would be to provide the light sheet in the sample through the same objective lens that is used for imaging on a fluorescence microscope. In 2013 our group demonstrated on-chip single lens light sheet imaging by making use of a microfluidic chip with an integrated planar waveguide [13]. Excitation light was delivered into the chip by butt coupling of a fiber coupled laser to the planar waveguide. The excitation light then emerges as a wide but thin sheet of light in the measurement microchannel. While the contrast enhancement was shown to be beneficial for accurate nanoparticle tracking in suspension, the general use of this device for imaging purposes is limited due to the light sheet being fixed in space. Galland et al. instead recently developed microfluidic sample holders with integrated reflective micromirrors which allow horizontal reflection of the excitation light sheet after it passes through the microscope's objective lens [14]. Such a design is compatible with high NA objective lenses and only requires appropriate beam shaping, which can be done before the laser beam is sent into the microscope body. The sample holders are made of a UV-curable polymer, index matched with the cell medium, and are obtained through replication from a silicon wafer with tilted microchannel walls prepared by anisotropic wet etching and dry etching.

Here we evaluated if a less complicated approach could be used to fabricate micromirrors. The process starts from an inexpensive PI wafer which is polished at 45° , cut in smaller parts and attached to a microscope slide. We achieved an on-chip light sheet thickness of $2.3\ \mu\text{m}$ (FWHM) at 638 nm for the polymer micromirrors, which was slightly worse than the $1.7\ \mu\text{m}$ (FWHM) at 638 nm for micromirrors prepared in silicon by anisotropic wet etching. However, the optical quality of replicated sample holders was better for those prepared from the polymer master mold as compared to those prepared from the silicon master mold. This shows that our approach based on an inexpensive polished polymer plugs is very well suited for upscaling of sample holders with integrated micromirrors for single-lens LSM. The suitability of those replicated sample holders for LSM microscopy was demonstrated by imaging breast cancer spheroids.

Such disposable sample holders with integrated micromirrors allow single-lens light sheet microscopy on chip. As it only requires minor modifications in the light path between the laser and the microscope body, the technique can be readily implemented on any research grade epi-fluorescent microscope and should allow the transfer of this technology to less

specialized laboratories. In summary, we proposed and tested a different approach to fabricate sample holders with integrated micromirrors for single-lens light sheet microscopy. The master mold obtained by polishing of an inexpensive polymer wafer was compared to a previously reported master mold obtained by anisotropic Si etching. While the optical quality of the Si master mold was slightly better than that of the polished polymer wafer, replica's from the latter made from UV-curable epoxy turned out to have the best performance. The usability of those replica's was demonstrated by capturing high-quality images of human cancer spheroids. Taken together our work shows that single lens LSM has the potential to become an accessible imaging modality that is compatible with standard fluorescence microscopes available in most cell biology labs.

Appendix A – Fabrication of sample holders

Fabrication procedure of silicon master mold

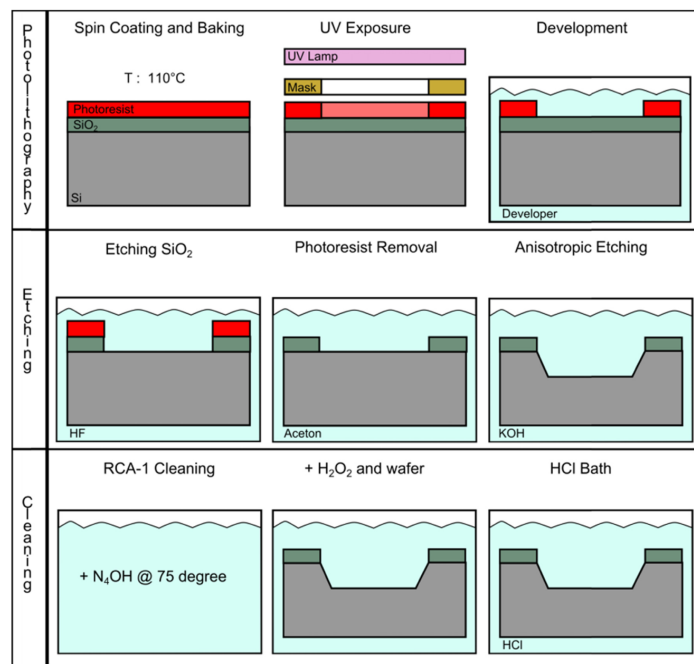


Fig. 8. Fabrication procedure of the silicon based master mold. The process is divided in three parts, namely photolithography, etching and cleaning. A thermo-oxidized wafer (silicon dioxide layer: $1\ \mu\text{m}$ thick) is spin coated with a primer and subsequently with a positive photoresist, both followed by a 3 minutes baking step at 110°C . Afterwards, the wafer is covered with a chrome mask, that defines the position of the tilted walls and the channel, and subsequently exposed to UV light for 200 seconds. The wafer is immersed for 90 s in an aqueous solution consisting of 1 part Developer 400K and 2 parts distilled water in order to remove the UV illuminated regions of the photoresist. In the subsequent etching step, the wafer is placed for 16 min into a buffered 7:1 HF solution that dissolves the unprotected regions of the silicon dioxide and exposes the underlying bare silicon. Next, the wafer is placed for 5 min in an ultrasonic bath filled with acetone to remove the photoresist layer. Then the wafer is put into a stirred KOH bath (KOH/Water/IPA 20/64/16) at 70°C that will selectively remove silicon in the $\langle 100 \rangle$ crystal direction, thus etching the channel with tilted walls at approximately $40\ \mu\text{m}/\text{hour}$. A careful monitoring of the etch rate by means of temperature and concentration of the etchant is of utmost importance since the etch rate can influence the wall roughness. Finally an RCA-1 clean was performed as follows. A solution of 5 parts water, 1 part 27% ammonium hydroxide and 1 part 30% hydrogen peroxide is heated at 70°C , then the wafer is soaked in the solution for 15 min, rinsed with water and put for 5 min into a 5% HCl solution.

Fabrication procedure of polymer master mold

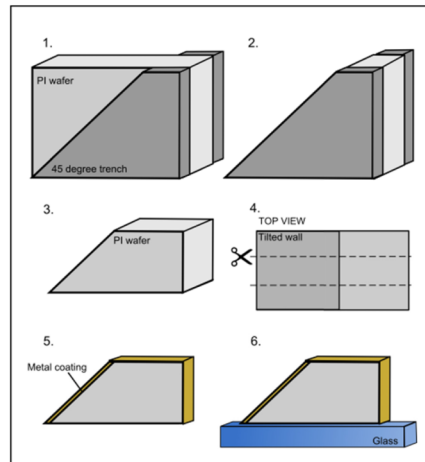


Fig. 9. Fabrication procedure of the polymer-based master mold. 1. A 500- μm -thick flexible PI wafer is clamped in a special PMMA device with a 45° trench. 2. The device is polished to provide a 45° polished end facet to the PI wafer. 3. The wafer is polished and thinned down at both sides to the desired thickness. This step also removes unwanted edge defects. 4. The wafer is cut into small parts of the desired length and width by a wafer dicer with a diamond coated blade. 5. The tilted end facets are then coated with a 120-nm-thin gold layer by vapor deposition, or with an aluminium layer applied by sputtering. 6. The polymer plug is now ready to be glued to a microscopy slide.

Replication process

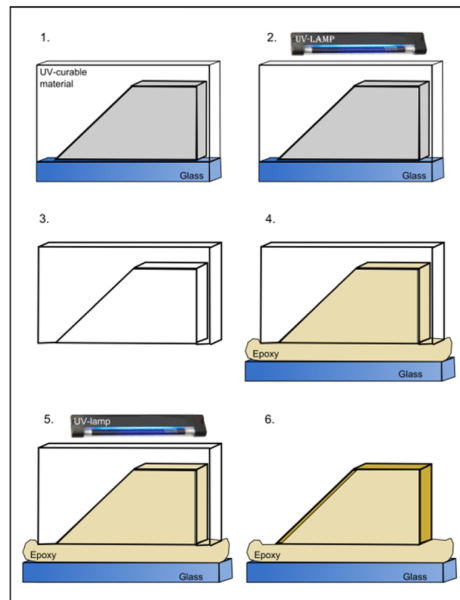


Fig. 10. Schematic overview of the replication process. 1. The polymer or silicon based master components are covered with a UV-curable, transparent fluorinated molding material. 2. The molding material is polymerized by UV illumination. 3. The polymerized mold is easily peeled off from the master component. 4. The material is used as a stamp to fabricate the actual replicas. A drop of a UV-curable epoxy is thus dispersed on a glass slide and the molding stamp is peeled off. 6. The replicated micromirrors are coated with a 200 nm reflective layer of either gold (evaporation) or aluminum (sputtering).

Appendix B – Metal coating

Comparison between metal coatings

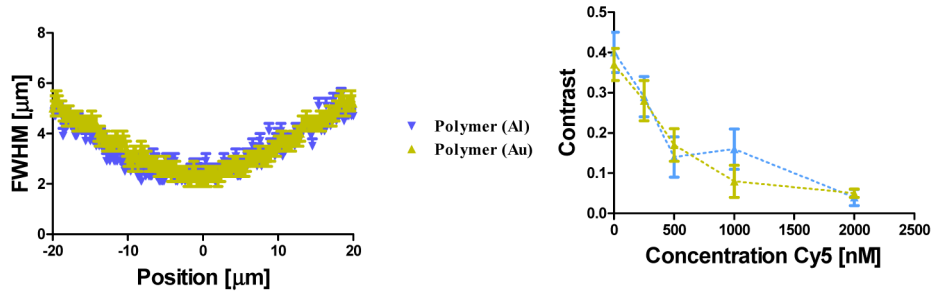


Fig. 11. Influence of metal coating on the beam profile (left) and on the contrast (right). Two polymer master molds were considered, one coated with aluminum through sputtering, the second coated with gold through evaporation. The beam profile was determined as described in the main text (section 4.1) and in Fig. 4. Contrast was determined for fluorescent nanospheres suspended in solutions with increasing concentration of the red fluorescent dye Cy5. Measurements were performed in both molds and compared with normal epi-fluorescence imaging. Neither the beam profile nor the contrast seem effected by the metal used for coating the micromirror.

Funding

Agency for Innovation by Science and Technology in Belgium (IWT); Ghent University Special Research Fund; Fund for Scientific Research Flanders (FWO, Belgium).